Accuracy of linear measurements from imaging plate and lateral cephalometric images derived from cone-beam computed tomography

Mazyar Moshiri,[a] William C. Scarfe,[b] Michael L. Hilgers,[c] James P. Scheetz,[d] Anibal M. Silveira,[e] and Allan G. Farman[f]

Louisville, Ky, and Phoenix, Ariz

Introduction: As orthodontic practice moves toward 3-dimensional cephalometric analyses, a solution is required to ensure sustained availability of well-established projected treatment outcomes based on 2-dimensional analyses. This ex-vivo study was conducted to compare the accuracy of linear measurements made on photostimulable phosphor cephalograms with 3 methods for simulating lateral cephalograms with cone-beam computed tomography (CBCT). **Methods:** The linear distances between anatomical landmarks on dentate dry human skulls were measured by observers using digital calipers for S-N, Ba-N, M-N, ANS-N, ANS-PNS, Pog-Go, Go-M, Po-Or, and Go-Co. The skulls were imaged with CBCT with a single 360° rotation, producing 306 basis images and achieving 0.4 mm isotrophic voxel resolution on volumetric reconstruction for making ray-sum reconstructed cephalograms. Two other cephalogram approaches were used with the CBCT system—a single transmission image generated as a scout image designed to check patient positioning before CBCT, and a single-frame lateral basis image. Conventional digital lateral cephalograms (LCs) were acquired with the photostimulable phosphor system. Images were imported into a cephalometric analysis program (Dolphin Imaging Cephalometric and Tracing Software, Chatsworth, Calif) to compute the included linear measurements. Analyses were repeated 3 times and statistically compared with measured anatomic truth with ANOVA ($P \leq .05$). The intraclass correlation coefficient was determined as an index of intra- and interobserver reliability. **Results:** The intraclass correlation coefficient for the LCs was significantly less than for the measured anatomic truth and for all CBCT-derived images. CBCT images either produced with individual frames or reconstructed from the volumetric data set were accurate for all measurements except Pog-Go and Go-M. CBCT scout images had the second highest accuracy for all measurements except Pog-Go, Go-M, and Go-Co. Conventional LCs had the least accuracy; they were accurate only for Po-Or and ANS-N. **Conclusions:** CBCT-derived 2-dimensional LCs proved to be more accurate than LCs for most linear measurements calculated in the sagittal plane. No advantage was found over single-frame basis images in using ray-sum generated cephalograms from the CBCT volumetric data set. (Am J Orthod Dentofacial Orthop 2007;132:550-60)

Radiographic imaging is an important diagnostic adjunct in the assessment of skeletal and dental relationships for the orthodontic patient. Since 1931, 2-dimensional (2D) planar images, made with standardized projection geometries, have been used to identify specific anatomic landmarks from which vertical and anteroposterior skeletal and dental dimensions can be derived. Recently, cone-beam computed tomography (CBCT) systems have been developed specifically for the maxillofacial region.[1-4] CBCT systems approved for use in the United States include the NewTom QR DVT 3G (Quantitative Radiology, Verona, Italy), CB MercuRay (Hitachi Medical, Chibaken, Japan), i-CAT (Imaging Sciences International, Hatfield, Pa), Iluma (Imtec Imaging, Ardmore, Okla), and 3D Accu-i-tomo-XYZ Slice View Tomograph, (J. Morita, Kyoto, Japan). All but the latter can image the skull to include most anthropometric landmarks used in cephalometric analysis.

CBCT uses rotational scanning by an x-ray source and a reciprocating x-ray detector to facilitate acquisition of many single projection frame basis images (Fig 1). CBCT allows 2D multi-planar reformatting (MPR)

[a]Graduate student, School of Dentistry, University of Louisville, Louisville, Ky.
[b]Associate professor, Division of Radiology and Imaging Sciences, Department of Surgical and Hospital Dentistry, School of Dentistry, University of Louisville, Louisville, Ky.
[c]Private practice, Phoenix, Ariz.
[d]Professor, Department of Diagnostic Sciences, Prosthetic and Restorative Dentistry, School of Dentistry, University of Louisville, Louisville, Ky.
[e]Associate professor, Department of Orthodontic and Pediatric Dentistry, School of Dentistry, University of Louisville, Louisville, Ky.
[f]Professor, Division of Radiology and Imaging Sciences, Department of Surgical and Hospital Dentistry, School of Dentistry, University of Louisville, Louisville, Ky.
Reprint requests to: William C. Scarfe, Department of Surgical and Hospital Dentistry, University of Louisville School of Dentistry, 501 S Preston St, Louisville, KY 40202; e-mail, wcscar01@louisville.edu.
Submitted, March 2006; revised and accepted, September 2006.
0889-5406/$32.00

doi:10.1016/j.ajodo.2006.09.046

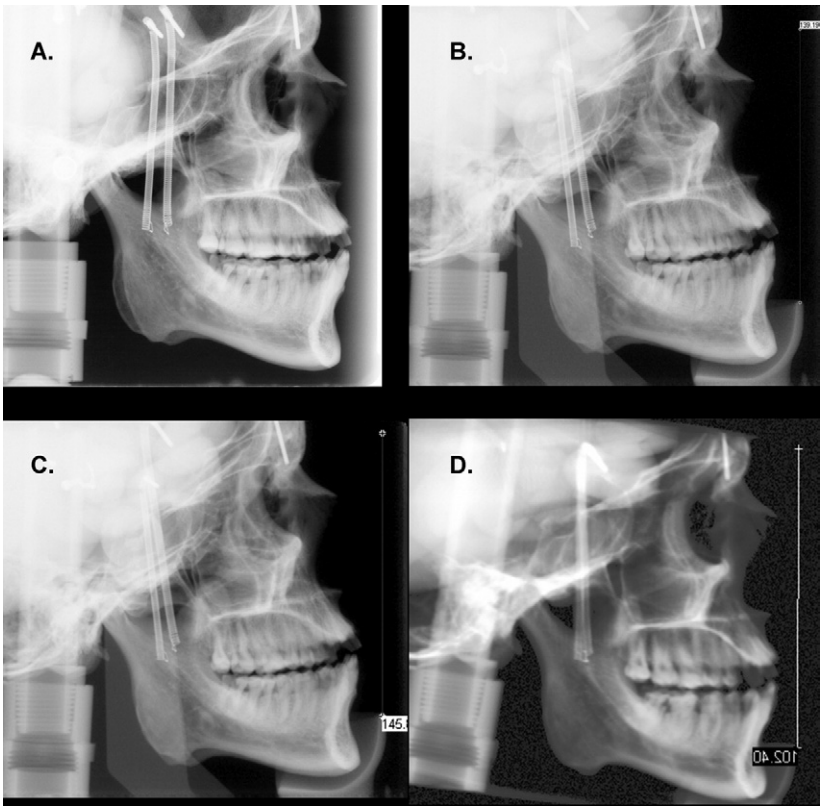

Fig 1. Selection of CBCT basis images: 4 basis image frames from 306 that comprising primary data for iCAT CBCT full scan. **A,** Frame 1, first basis projection image; **B,** frame 75; **C,** frame 152; **D,** frame 306, last basis image.

and secondary reconstruction of the data in a personal computer, thereby allowing generation of images in orientations other than the conventional axial plane. Time and dose requirements were suggested to be similar to other dental radiographic modalities in present use.[2,5-9] Maxillofacial applications of CBCT have been used for maxillofacial surgery,[10-14] implantology,[15-18] and orthodontics.[19-24] High dimensional accuracy has been reported for CBCT in measurement of facial structures.[18,25-31]

Cephalograms have been used in orthodontic treatment planning and outcomes assessments for 75 years. Over this time, a substantial database of information linking 2D standardized head radiographs to orthodontic treatment outcomes has been collected. As the orthodontic specialty moves toward the use of a 3-dimensional (3D) cephalometric paradigm, it seems illogical to discard the valuable information from the past. There might well be a value to be able to reconstruct classical cephalograms from a CBCT data set without the need to unnecessarily reirradiate the patient. Ray-sum MPR (Fig 2) has been reported to be a potential method to simulate lateral cephalometric images from CBCT data sets.[32-35] The ray-sum approach has been termed the "virtual cephalogram"[33]; however, this term could be considered ambiguous because it is not specific semantically to 2D or to ray-sum approaches. To date, there has been no systematic quantification of the precision of the ray-sum approach to 2D cephalometry.

An alternative to the ray-sum approach could be simply to use the CBCT detector as a digital panel for a more traditional cephalogram projection but with shorter source-to-patient and greater patient-to-detector distances than are usual for traditional cephalography. Chidiac et al[36] used scout images from a medical computed tomography system for this purpose. Similar scout images are used for checking patient positioning before a CBCT volume scan. Furthermore, if a single-frame basis image is sufficient to replicate information needed for traditional cephalometry, the number of frames would be reduced to approximately 1 in 300, with substantial savings in dose to the patient if a volumetric data set analysis is not required.[38]

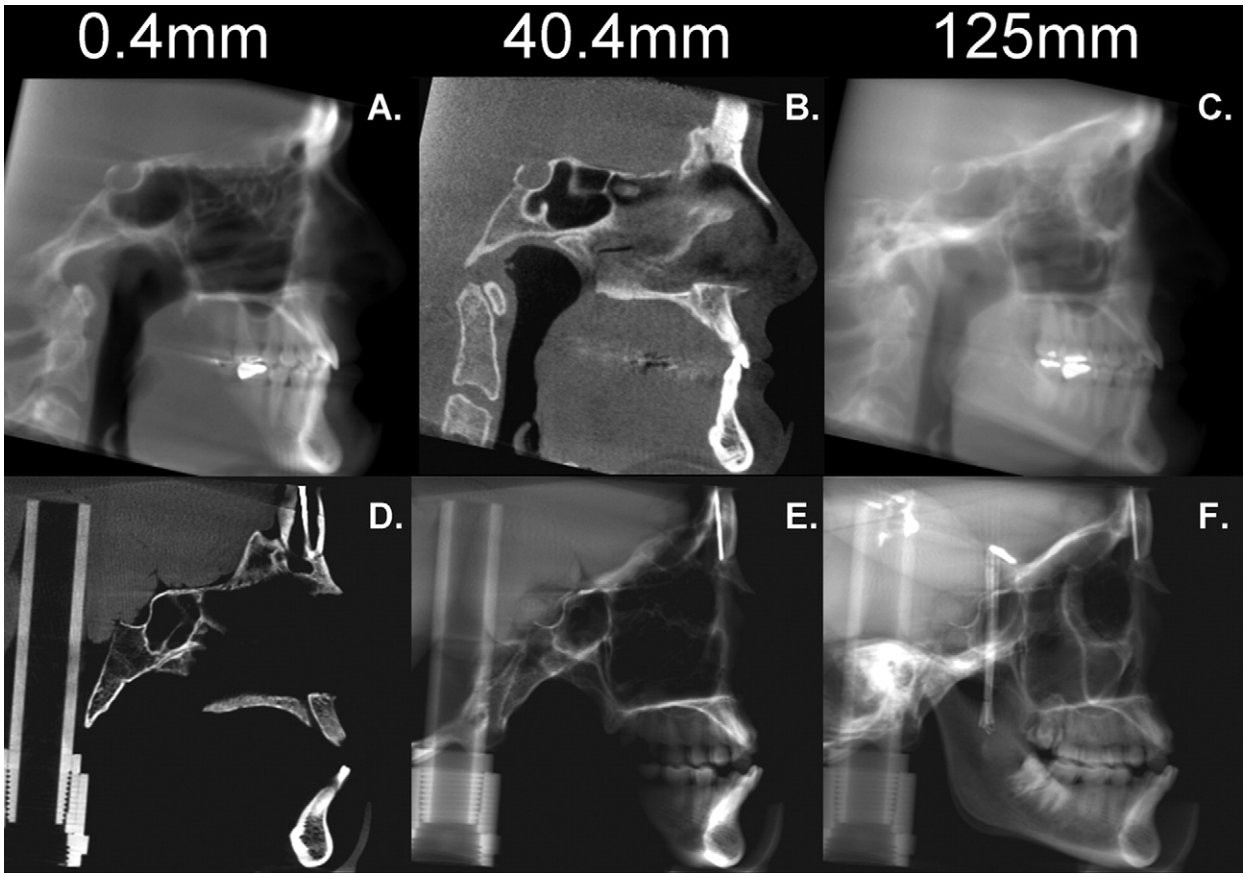

Fig 2. Example of construction of 2D ray-sum simulated cephalometric image using **A-C,** patient data and **D-F,** dry skull sample demonstrating similarity in both hard- and soft-tissue representations of conventional cephalograms. Construction of lateral simulated 2D cephalometric images from gradual increase in sagittal reference plane thickness (left to right) 0.4, 40, and 125 mm, respectively.

The purpose of this study was to quantify the cephalometric measurement accuracy of cephalograms derived from CBCT by using a ray-sum approach, of CBCT scout images, and of CBCT single-frame basis images compared with traditional cephalograms captured on photostimulable phosphor (PSP) and to anatomic truth.

MATERIAL AND METHODS

This ex-vivo experiment with dry human skulls was approved by the Institutional Human Remains Committee, Department of Anatomical Sciences and Neurobiology, at the University of Louisville. The sample comprised 23 dry skulls with full permanent dentition and stable and reproducible occlusion. No demographic data was available; the skulls were not identified by age, sex, or ethnicity. Fifteen anatomical landmarks, of which 4 were bilateral, were identified by consensus on each skull by using an indelible marker (Table I). The distances between these landmarks provided 9 linear dimensions commonly used in lateral cephalometric analysis (Fig 3). To establish the true distances between the selected anatomic points, measurements were independently made 3 times each by 2 observers (M.M. and W.C.S.) using an electronic digital caliper (27-500-90; GAC, Bohemia, NY). The mean of the 6 measurements was the anatomic truth. The left and right measurements for the bilateral linear dimensions (Pog-Go, Go-M, Po-Or, and Go-Co) were averaged.

To provide soft-tissue equivalent attenuation, 2 latex balloons filled with water were placed in the cranial vault before imaging. To separate the mandibular condyle from the temporal fossa, a 1.5-mm thick expanded rigid polystyrene plastic wedge was placed in the joint space between the glenoid fossa and the condylar head. For all images, the teeth were placed in

Table I. Definition of anthropometric landmarks in cephalometric analysis

Landmark (abbreviation)	*Definition*
Sella (S)	Midpoint of rim between anterior clinoid process in median plane
Nasion (N)	Midsagittal point at junction of frontal and nasal bones at nasofrontal suture
Orbitale* (Or)	Most inferior point on infraorbital rim
Anterior nasal spine (ANS)	Most anterior limit of floor of nose, at tip of ANS
Posterior nasal spine (PNS)	Point along palate immediately inferior to pterygomaxillary fossa
Pogonion (Pog)	Most anterior point along curvature of chin
Menton (M)	Most inferior point along curvature of chin
Gonion* (Go)	Point along angle of mandible, midway between lower border of mandible and posterior ascending ramus
Basion (Ba)	Most inferior point on anterior margin of foramen magnum, at base of clivus
Porion* (Po)	Most superior point of anatomic external auditory meatus (anatomic Po)
Condylion* (Co)	Most posterior superior point of midplaned contour of mandibular condyle

*Bilateral landmark.

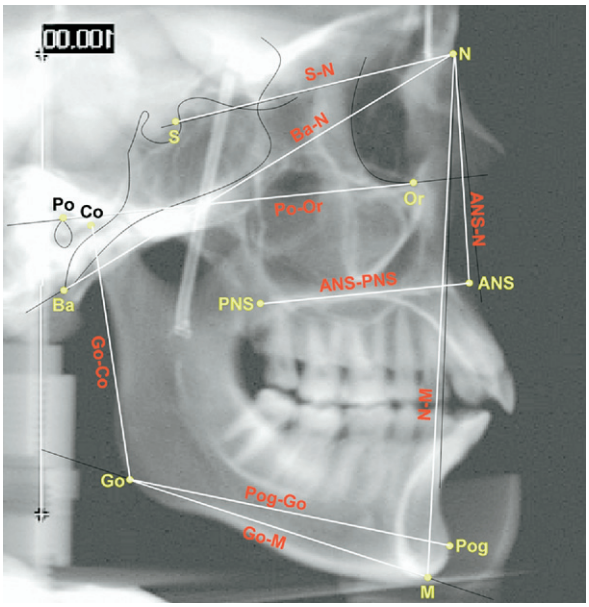

Fig 3. Anatomic landmarks and planes used in analysis superimposed on representative 2D ray-sum simulated lateral cephalometric image generated from skull. Linear distances were determined for the following dimensions: *S-N,* sella-nasion; *Ba-N,* basion-nasion; *N-M,* nasion-menton; *ANS-N,* anterior nasal spine-nasion; *Pog-Go,* pogonion-gonion; *Go-M,* gonion-menton; *ANS-PNS,* anterior nasal spine-posterior nasal spine; *Po-Or,* porion-orbitale; *Go-Co,* gonion-condylion.

centric occlusion (maximum intercuspation), and the jaws were held closed by bilateral metal springs. A custom plastic head holder, with a polyvinyl chloride pipe extension to place in the foramen magnum, was constructed to support the skulls during imaging.

Two modalities were used to image the skulls. CBCT images were acquired with the i-CAT system, operated at 3 to 8 mA (pulse mode) and 120 kV with a high-frequency generator with fixed anode and 0.5 mm nominal focal spot size. The anterior symphyseal region of the mandible of each skull was placed in the chin holder, and vertical and horizontal lasers were used to position the skull. Each specimen was oriented by adjustment of the chin support until the midsagittal plane was perpendicular to the floor, and the horizontal laser reference coincided with the intersection of the posterior maxillary teeth and the alveolar ridge. Lateral scout images were made, and head position was adjusted so that discrepancies between bilateral structures (eg, posterior and inferior borders of the mandibular rami and zygomatic arches) were less than 5 mm. A single 360° rotation, 20-second scan, comprising 306 basis projections was then made of each skull with a 17.0 cm (diameter) x 13.2 cm (height) field of view with the i-CAT acquisition software (version 1.7.7). Control of acquisition parameters (mA, kVp) was automated. Primary reconstruction of the data, automatically performed immediately after acquisition, took approximately 60 seconds. Secondary reconstruction occurred in real time and provided contiguous color-correlated perpendicular axial, coronal, and sagittal 2D MPR slices, with isotropic 0.4-mm voxels. Three methods were used to create 2D simulated lateral skull projection images with the CBCT system: (1) the scout method involved the export of the final lateral scout radiograph originally made to confirm positioning; (2) the basis frame method involved the selection of a basis image with the least anatomic discrepancy between the right and left sides corresponding to a lateral cephalometric projection; and (3) the ray-sum technique involved generation of the image by using the entire volumetric data set as previously described.[32-35] A simulated 2D lateral cephalogram can be produced by adjusting the sagittal reference plane on the axial image to coincide with the midpoint of the sella turcica, bisecting the foramen magnum, and increasing the slice thickness of this plane to a width of approximately 130

Table II. Features of imaging plate and CBCT digital images

Image		Image dimensions (width × height)		Image			
Modality	Type	Matrix size (pixels)	Physical size (in)	File size (kB)	dpi	Calibration factor	Final dpi
Projection radiograph	Lateral cephalometric	2847 × 2386	9.5 × 7.96	6804	300	9.92%	327
CBCT	Scout	960 × 768	13.33 × 10.67	759	72	0%	72
	Frame	480 × 384	6.67 × 5.33	206	72	0%	72
	Reconstructed	476 × 330	6.57 × 4.58	178	72	−12.5%	63

to 150 mm. This provides an image composed of the summed voxels—the ray-sum image (Fig 3).The window and leveling of these images were adjusted to a standard window (3000/300, respectively). No enhancement filters were used.

Traditional lateral cephalography was performed with a Quint Sectograph (model QS 10-1627W; Denar, Anaheim, Calif) and 10:1 parallel grid. The source-to-midsagittal plane distance was maintained at 150 cm. The detector was positioned 15 cm from the midsagittal plane for all exposures. Exposure settings were 78 kVp, 200 mA, and 2/15 seconds. For the lateral cephalogram (LC), the skull was stabilized by 2 ear rods in the external auditory meati and positioned with the Frankfort plane parallel to the floor, the sagittal plane perpendicular to the x-ray beam, and the left side closest to the detector. The central ray was directed at the right external auditory meatus.

Digital transmission images were acquired by using an 8 x 10-in photostimulable storage phosphor imaging plate (Gendex, Des Plaines, Ill). Exposure parameters were determined by subjective evaluation of image quality of many images at various exposures on a skull with a 1-cm thick Perspex attenuation material (Lucite International, Southampton, United Kingdom) over the exit beam. The plates were scanned at 300 dpi and saved in 16-bit tagged image file format (TIFF) by using the DenOptix imaging system (Gendex). The images were equalized and despeckled with proprietary software (VixWin 2000, version 1.2; Gendex). CBCT images were acquired with a 1024 × 1024 matrix hydrogenated amorphous silicon flat-panel detector with cesium iodide scintillator and stored as DICOM files. CBCT reconstructed images were reformatted from 306 basis projections, providing a cubic voxel size of 0.4 mm.

Specific CBCT images were selected, imported into PhotoShop software (version 7.0; Adobe Systems, San Jose, Calif) and saved as 8-bit TIFF images. CBCT scout and single basis image LCs were inverted to produce black backgrounds. Traditional LC images were exported from VixWin 2000 software and saved as 8-bit TIFF images. The resulting image matrix dimensions, image sizes, resolutions, and file sizes varied depending on the modality (Table II). Images were imported into a cephalometric analysis program (Dolphin Imaging Cephalometric and Tracing Software, Chatsworth, Calif). Because of differences in image dimensions and dpi, separate calibration was necessary for each image modality. Therefore, a 100-mm radiographic film calibration ruler (model PN 130-0168; Dolphin Imaging Cephalometric and Tracing Software) was placed in the midsagittal plane of a skull perpendicular to the radiographic beam for each modality and imaged. These images were used to calculate the image-casting magnification factor for each modality and calibrate distances measured in the cephalometric analysis program. The calculated calibration magnification factors and resulting dpi used in the software program are shown in Table II.

The images were coded and viewed on a 17-in flat panel color active matrix TFT (Dell E171FPb Flat Panel Color Monitor; Dell, Round Rock, Tex) monitor screen having a resolution of 1024 × 768 at 60 Hz and a 0.264 mm dot pitch, operated at 32-bit color. A custom analysis in the program was developed to direct the observer to identify specific anatomic landmarks on the images (Table I). Landmarks were identified by using a cursor-driven pointer. The analysis provided specific linear measurements (Fig 3) that were exported as text data. Some anatomic landmarks required identification of bilateral structures that are inherently difficult to view on conventional cephalograms. For those points, the observer was instructed to attempt to differentiate between left and right features and construct a point midway between them. If the feature could not be differentiated, the right and left condyle landmarks were considered coincident. Although theoretically this would lead to differential magnification of left- and right-sided condylar images compared with the midsagittal correction factor, the minimal influence on absolute dimension in relation to the size of the

Table III. ICC for triplicate measurements of 2 raters for midsagittal and bilateral linear measurements of 23 skulls

Linear dimension	Location	Rater 1			Rater 2		
		95% Confidence interval			95% Confidence interval		
		Mean	Lower	Upper	Mean	Lower	Upper
S-N	Midsagittal	0.9845	0.9694	0.9929	0.9905	0.9811	0.9956
Ba-N	Midsagittal	0.9877	0.9756	0.9944	0.9847	0.9697	0.9930
PNS-ANS	Midsagittal	0.9728	0.9465	0.9875	0.9824	0.9653	0.9919
Na-A	Midsagittal	0.9912	0.9826	0.9960	0.9915	0.9831	0.9961
Na-M	Midsagittal	0.9953	0.9906	0.9978	0.9756	0.9519	0.9888
Na-B	Mid-sagittal	0.9947	0.9895	0.9976	0.9977	0.9955	0.9990
N-ANS	Midsagittal	0.9763	0.9533	0.9891	0.9916	0.9833	0.9962
14-3	Midsagittal	0.9733	0.9475	0.9877	0.9886	0.9773	0.9948
Pog-Go	Right	0.9975	0.9950	0.9988	0.998	0.9959	0.9991
Pog-Go	Left	0.9987	0.9973	0.9994	0.9996	0.9993	0.9998
Pog-Co	Right	0.9960	0.9921	0.9982	0.997	0.9941	0.9987
Pog-Co	Left	0.9945	0.9889	0.9975	0.9487	0.9008	0.9762
Go-M	Right	0.9961	0.9923	0.9982	0.9988	0.9976	0.9994
Go-M	Left	0.9667	0.9349	0.9846	0.9992	0.9984	0.9996
Po-Or	Right	0.9893	0.9787	0.9951	0.9889	0.9779	0.9944
Po-Or	Left	0.9897	0.9795	0.9953	0.9900	0.9801	0.9954
Go-Co	Right	0.9951	0.9902	0.9977	0.9956	0.9912	0.998
Go-Co	Left	0.9969	0.9938	0.9986	0.9976	0.9951	0.9989
Mean		0.9887			0.9898		
SD		0.0099			0.0122		

No significant difference between raters: Student paired *t* test: $P = .77$.

feature and the summation of these distances averaged the effect.

Statistical analysis

All data were entered into Microsoft Excel 2004 (Microsoft, Redmond, Wash). Means and standard deviations of 3 independent repeats from the 2 observers of the 9 measurements were calculated for each skull and defined as anatomic truth. For each imaging mode, the average of 3 independent analyses was used. The data files were coded for use with the Statistical Package for the Social Sciences (version 12.0; SPSS, Chicago, Ill). To determine intraobserver precision, the intraclass correlation coefficient (ICC) was determined. With the Student *t* test, the ICC was compared between the 2 raters measuring skull dimensions. If no differences existed between raters, the ICC was then averaged for both raters and between sides. Modality differences were compared with 1-way ANOVA by using the Scheffé post-hoc analysis. Modality measurement dimensions were determined to be distributed normally by the Levene statistic, so the mean of the 3 repeat measurements was used in the analysis. The statistical methods consisted of 1-way ANOVA for each measurement dimension at an à priori level of significance of $P = .05$. The post-hoc survey was the Tukey HSD.

RESULTS

Table III shows the ICC for each rater and linear distance measured 3 times on the skull. The Student *t* test ($P = .77$) did not show significant differences in precision between raters; therefore, the 2 raters' ICCs were averaged to provide a single ICC. For bilateral dimensions, the average ICC was determined by averaging the left and right measurements of both raters.

Table IV gives the averaged ICCs of 3 skull dimensions by 2 raters compared with 3 orthodontic linear measurements by 1 rater for each plane for LC vs CBCT 2D lateral cephalograms. ANOVA indicated differences in ICCs between groups ($F = 18.54$, $P < .0001$). The reliability of repeated skull measurements was significantly greater than for any repeated modality measurement except frame derived CBCT ($P = .25$). The reliability of repeated measurements on LCs was significantly less than all CBCT modalities.

Table V lists the measured mean dimensions for each plane distance compared with those obtained from CBCT cephalometric images and LCs. For all 5 median sagittal dimensions (S-N, Ba-N, M-N, ANS-N, and ANS-PNS), CBCT-derived values did not differ from actual dry skull dimensions, whereas, for 4 of the five measurements (S-N, Ba-N, M-N, and ANS-PNS), the LC measurements were significantly higher. For

Table IV. ICC of triplicate skull dimensions by 2 raters compared with triplicate orthodontic linear measurements by 1 rater for each cephalometric plane for conventional imaging plate based and CBCT-derived 2D simulated lateral cephalometric projections.

	Modality				
	*Truth**	*Imaging plate*	*CBCT*		
Linear dimension	*Skull*	*Lateral cephalometric*	*Scout*	*Frame*	*Reconstructed*
S-N	0.9875	0.6215	0.9093	0.9421	0.8712
Ba-N	0.9862	0.5693	0.8212	0.9138	0.8934
N-M	0.9855	0.7673	0.9858	0.9848	0.9498
ANS-N	0.9839	0.5495	0.9491	0.9319	0.7605
ANS-PNS	0.9776	0.6955	0.7731	0.7922	0.8173
Pog-Go†	0.9985	0.7763	0.8500	0.9285	0.9456
Go-M†	0.9902	0.8461	0.8063	0.9077	0.9133
Po-Or†	0.9895	0.7519	0.7971	0.9138	0.9187
Go-Co†	0.9963	0.8428	0.8448	0.8750	0.8459
Means ± SD	0.9884 ± 0.00632‡	0.7134 ± 0.111§	0.8596 ± 0.073	0.9099 ± 0.0531	0.8795 ± 0.0626

*Mean value from measurements of 2 raters.
†Mean value from measurements of both sides.
‡Significant difference between skull and imaging plate lateral cephalometric and all CBCT modalities except frame derived.
§Significant difference between imaging plate lateral cephalometric and skull and all CBCT modailities.

Table V. Mean length (mm ± SD) of orthodontic linear dimensions for each cephalometric plane for conventional digital and CBCT-derived simulated lateral cephalometric projections

	Modality					*Significance*	
	Truth	*Imaging plate*	*CBCT*				
Dimension	*Skull*	*Lateral cephalometric*	*Scout*	*Frame*	*Reconstructed*	*F value*	*P*
S-N	59.49 ± 3.62	64.94 ± 3.00†	60.95 ± 2.92	60.78 ± 3.18	61.27 ± 2.82	9.88	.000
Ba-N	98.07 ± 5.7	104.98 ± 5.52†	98.14 ± 4.82	97.98 ± 5.12	99.72 ± 4.46	7.78	.000
N-M	109.24 ± 6.85	116.81 ± 7.57†	109.81 ± 7.22	109.03 ± 6.85	110.43 ± 7.11	4.69	.002
ANS-N	46.64 ± 2.77	48.79 ± 2.71‡	45.84 ± 2.54	45.19 ± 2.94	46.41 ± 2.58	5.79	.000
ANS-PNS	47.61 ± 3.23	50.5 ± 4.56†	45.93 ± 3.32	46.12 ± 3.53	46.73 ± 2.71	6.48	.000
Pog-Go*	83.34 ± 7.69c	77.94 ± 6.57	74.78 ± 6.03	73.36 ± 5.71	74.9 ± 6.26	8.68	.000
Go-M*	79.37 ± 5.64§	74.49 ± 6.29	72.05 ± 6.08	70.55 ± 5.57	71.50 ± 5.82	8.16	.000
Po-Or*	78.22 ± 4.74	79.44 ± 5.34	77.69 ± 4.71	77.83 ± 5.6	76.16 ± 4.00	1.33	.27
Go-Co*	56.49 ± 5.09	59.36 ± 6.56‡	51.3 ± 4.59¶	52.46 ± 5.01	54.74 ± 4.48	8.8	.000

*Mean value from measurements of both sides.
†Significant difference from actual skull measurement and all CBCT-derived dimensions.
‡Significant difference from all CBCT-derived dimensions only.
§Significant difference of actual measurement from lateral cephalometric and all CBCT-derived dimensions.
¶Significant difference from actual dimensions.

ANS-N, although the LC and CBCT modalities were significantly different, they were not different from the actual dry-skull dimensions. Of the 3 bilateral measurements, only Po-Or provided measurements similar to the actual dry-skull dimensions with no differences between modalities. For Pog-Go and Go-M, all modalities provided significantly smaller measurements from the actual dimensions with no differences between modalities. For Go-Co, measurements from the CBCT scout images were significantly less than the actual dimensions. In addition, for Go-Co, LC measurements were significantly higher than all CBCT-derived measurements but were not significantly different from actual measurements.

DISCUSSION

No single imaging technique has been readily available to provide an accurate, easily interpreted

representation of all osseous aspects of the craniofacial region in 1 exposure. Previously, a plain LC, occasionally combined with a coronal (posteroanterior) or axial (submentovertex) projection, was used for visualization of jaw symmetry or asymmetry. The rapidly emerging availability of maxillofacial CBCT allows clinicians to reformat the volumetric data set for conventional (scout, basis frame) or ray-sum wide-slice sections simulating plane projections such as cephalometric, submentovertex, and posteroanterior views—all with 1 relatively short scan.

We compared the accuracy of linear measurements made on PSP cephalograms with 2D LCs derived from volumetric reconstruction CBCT data sets. We found that CBCT images either produced with individual frames or reconstructed from the volumetric data set were accurate for all measurements except Pog-Go and Go-M. CBCT scout images had the second highest accuracy for all measurements except Pog-Go, Go-M, and Go-Co. Conventional LCs had the least accuracy; they were accurate only for Po-Or and ANS-N. Our results differ with those of Chidiac et al,[36] who found reduced correlation to skull dimensions for transverse measuresments for scout images of a medical fan-beam computed tomography compared with conventional cephalograms.

There was a trend for our lateral cephalometric measurements to be statistically significantly greater than the skull measurements in 4 of the 5 midsagittal (S-N, Ba-N, N-M, ANS-PNS) and in 1 of the 4 bilateral (Go-Co) measurements. Magnification ranged from 4.6% to 9.1%. Although this discrepancy could be due, in part, to a previously reported systematic error specific to this software's calculation algorithm,[38] other potential sources of error include inherent differences in image acquisition, head position,[39,40] and linear projective transformation. [41,42] Adams et al[43] reported similar findings: certain midsagittal measurements (Na-Gn, Na-B, Na-S, Na-A, and A-B) were significantly greater than truth on 2D cephalograms (9.82, 8.32, 6.22, 4.99, and 3.11 mm, respectively). The interaction of these factors could also result in the significantly higher ICCs of repeated measurements on PSP LCs compared with those derived from CBCT.

The projection geometries of the 2 generators used in this study are intrinsically different. Conventional cephalographic systems, both film and digital, incorporate a long source-to-object distance, providing relatively parallel x-ray beam geometry resulting in an inherent differential magnification of bilateral structures. Although midsagittal structures are commonly magnified by as much as 10%, convention dictates that when bilateral landmarks are identified (eg, Or, Po, Go), location for analytical purposes is determined by visual approximation of the mental average of both positions. This introduces an inherent variability in the localization of these structures based on the observer's visual acuity. In comparison, CBCT incorporates a relatively short source-to-object distance with relatively divergent x-ray beam geometry, producing a projection with marked differential magnification. However, single-frame images are not based on image projection geometry alone. CBCT images are produced only after application of a reconstruction algorithm, such as that of Feldkamp et al.[44] Such algorithms incorporate geometric correction factors compensating for differential distortion peripheral to the central x-ray beam projection along with back projection corrections for tube position, tube, object, and detector distances. Resultant single CBCT images are therefore corrected to produce orthogonal projections with no differential magnification between bilateral or midsagittal structures. We believe that this correction accounts for the consistent and remarkable (<2 mm) accuracy of CBCT images for midsagittal linear dimensions, irrespective of derivation as compared with conventional lateral cephalometric images.

In addition to inherent x-ray projective beam geometry differences between techniques, many other potential sources of error contribute to the relative inaccuracy of conventional LCs.[45] These include head malpositioning,[39,40,46,47] radiographic method of analysis,[39] error due to landmark identification,[39] and intra- and interobserver errors.[48] The skulls were positioned in the cephalostat, and the Frankfort horizontal was adjusted visually before exposure compared with skull positioning in the CBCT equipment, which used laser level indicators. In addition, digital scout images were acquired to establish minimal bilateral discrepancy before final CBCT acquisition. We expected that the accuracy of the digital LCs might be greater than the CBCT-derived images because the former used PSPs processed at 300 dpi, substantially higher than the resolution used to screen capture CBCT images (72 dpi). However, investigators indicated no quantitative differences in mean error distances in lateral cephalometrics at resolutions as low as 75 dpi.[49,50]

The method of establishing anatomic truth could have contributed to bias in the results because, although the landmark identification and measurements on the radiographs were repeated, landmark identification on the skulls was done only once, albeit by consensus. This reduced the error of point identification on the skulls, but the establishment of a consensus landmark location was necessary to provide a fiducial reference to which we could compare the inherent clinical inaccu-

racies of both landmark identification and measurement associated with the radiographic technique.

Regarding bilateral measurement accuracy, it was expected that these would be smaller in overall dimensions because 3D linear distances (eg, Pog-Go) are projected onto a planar surface. This was generally true for all dimensions except Po-Or, for which we found no differences in accuracy between modalities. This was most probably because the deviation of this dimension from the midsagittal is minimal.

This study was limited in that soft tissue used for attenuation was minimal and consisted of a simulated water-based brain and separation of the condyle from the fossa with expanded rigid polystyrene plastic. No effort was made to simulate facial soft tissues because this would have increased structural noise and scatter radiation, potentially increasing the variability of landmark identification. The image accuracy of the CBCT images in this clinical simulation might have been reduced because of decreased signal-to-noise ratio due to scatter inherent in CBCT systems with increasing volumetric exposure.

It would be tempting, based on the greater accuracy of dimensions obtained with simulated cephalometric images generated from an entire CBCT volumetric data set, to interpret our findings as advocating this modality in orthodontic practice. Apart from greater accuracy, CBCT volumetric data sets can be reoriented so that reconstructed lateral ray-sum images produce simulated cephalometric images with optimal orientation. However, our results also indicate only a marginal advantage in the measurement accuracy of ray-sum reconstructions when compared with images generated from a single CBCT scout projection or single-frame basis image. In addition, we did not take into account comparative radiation exposures required to produce such images. A complete CBCT scan often requires about 300 successive basis image frame exposures. Because there were no differences in accuracy in the dimensions from a single-frame image and a reconstructed ray-sum image from 306 frames, this implies up to a 306-fold increase in exposure to produce a comparable LC. In addition, perhaps statistical differences producing conclusions of greater accuracy do not consider the clinical significance of our findings. Kamoen et al[45] provided absolute repeatability guidelines based on a 95% confidence interval for commonly used cephalometric variables and listed estimates of the minimal 99% critical difference in error for specific sample sizes. Although they did not provide guidelines for tolerances for their linear measurements, all measurement discrepancies between conventional lateral cephalometric and anatomic measurements were 2 to 5 mm, well within acceptable clinical tolerance.

Further studies are needed to investigate the clinical efficacy of CBCT-derived conventional projections by using the ray-sum reconstruction, particularly for patients with craniofacial asymmetry. In addition, clinical cost/benefit analyses incorporating exposure considerations should be made to assist in developing appropriate patient selection criteria for CBCT imaging in cephalometric analysis.[35] Nevetheless, our results indicate that CBCT manufacturers might consider permitting very low single-frame cephalograms in various orientations beyond the lateral scout image. Such images could act as a low-dose baseline. When 3D information is required (eg, to assess dental impactions), this could then be restricted to as narrow a field of view as required to obtain the necessary diagnostic information. Then very high spatial resolution can be applied.

CONCLUSIONS

For most 2D cephalometric measurements in the sagittal plane, simulated 2D lateral cephalometric projections from CBCT proved to be more accurate than conventional LCs. Although 2D cephalograms generated from single CBCT basis projections improved the accuracy of cephalometric measurements over conventional cephalography, there was no additional gain from using ray-sum images generated from the CBCT volumetric data set.[37]

We thank April Styles, our 2005 summer research associate and graduate student in oral biology, and Oana Bida Honey at the University of Louisville School of Dentistry for their valuable assistance in this project.

REFERENCES

1. Mozzo P, Procacci C, Tacconi A, Martini PT, Andreis IA. A new volumetric CT machine for dental imaging based on the cone-beam technique: preliminary results. Eur Radiol 1998;8:1558-64.
2. Hashimoto K, Arai Y, Iwai K, Araki M, Kawashima S, Terakado M. A comparison of a new limited cone beam computed tomography machine for dental use with a multidetector row helical CT machine. Oral Surg Oral Med Oral Pathol Oral Radiol Endod 2003;95:371-7.
3. Sukovic P. Cone beam computed tomography in craniofacial imaging. Orthod Craniofac Res 2003;6(Suppl 1):31-6.
4. Baba R, Ueda K, Okabe M. Using a flat-panel detector in high resolution cone beam CT for dental imaging. Dentomaxillofac Radiol 2004;33:285-90.
5. Bianchi S, Anglesio S, Castellano S, Rizzi L, Ragona R. Absorbed doses and risk in implant planning: comparison between spiral CT and cone-beam CT [abstract]. Dentomaxillofac Radiol 2001;30(Suppl 1):S28.

6. Schulze D, Heiland M, Thurmann H, Adam G. Radiation exposure during midfacial imaging using 4- and 16-slice computed tomography, cone beam computed tomography systems and conventional radiography. Dentomaxillofac Radiol 2004;33: 83-6.
7. Ludlow JB, Davies-Ludlow LE, Brooks SL, Howerton WB. Dosimetry of 3 CBCT devices for oral and maxillofacial radiology: CB Mercuray, NewTom 3G and i-CAT. Dentomaxillofac Radiol 2006;35:219-26.
8. Mah JK, Danforth RA, Bumann A, Hatcher D. Radiation absorbed in maxillofacial imaging with a new dental computed tomography device. Oral Surg Oral Med Oral Pathol Oral Radiol Endod 2003;96:508-13.
9. Tsiklakis K, Donta C, Gavala S, Karayianni K, Kamenopoulou V, Hourdakis CJ. Dose reduction in maxillofacial imaging using low dose cone beam CT. Eur J Radiol 2005;56:413-7.
10. Ziegler CM, Woertcher R, Brief J, Hassfeld S. Clinical indications for digital volume tomography in oral and maxillofacial surgery. Dentomaxillofac Radiol 2002;31:126-30.
11. Nakagawa Y, Kobayashi K, Ishii H, Mishima A, Ishii H, Asada K, et al. Preoperative application of limited cone beam computerized tomography as an assessment tool before minor oral surgery. Int J Oral Maxillofac Surg 2002;31:322-6.
12. Danforth RA, Peck J, Hall P. Cone beam volume tomography: an imaging option for diagnosis of complex mandibular third molar anatomical relationships. J Calif Dent Assoc 2003;31:847-52.
13. Heiland M, Schmelzle R, Hebecker A, Schulze D. Intra-operative 3D imaging of the facial skeleton using the SIREMOBIL Iso-C3D. Dentomaxillofac Radiol 2004;33:130-2.
14. Hamada Y, Kondoh T, Noguchi K, Iino M, Isono H, Ishii H, et al. Application of limited cone beam computed tomography to clinical assessment of alveolar bone grafting: a preliminary report. Cleft Palate Craniofac J 2005;42:128-37.
15. Hatcher DC, Dial C, Mayorga C. Cone beam CT for pre-surgical assessment of implant sites. J Calif Dent Assoc 2003;31:825-33.
16. Sarment DP, Sukovic P, Clinthorne N. Accuracy of implant placement with a stereolithographic surgical guide. Int J Oral Maxillofac Implants 2003;18:571-7.
17. Sato S, Arai Y, Shinoda K, Ito K. Clinical application of a new cone-beam computerized tomography system to assess multiple two-dimensional images for the preoperative treatment planning of maxillary implants: case reports. Quintessence Int 2004;35: 525-8.
18. Kobayashi K, Shimoda S, Nakagawa Y, Yamamoto A. Accuracy in measurement of distance using limited cone-beam computerized tomography. Int J Oral Maxillofac Implants 2004;19:228-31.
19. Mah JD, Hatcher D. Current status and future needs in craniofacial imaging. Orthod Craniofac Res 2003;6(Suppl 1):10-6.
20. Vannier MW. Craniofacial computed tomography scanning: technology, applications and future trends. Orthod Craniofac Res 2003;6(Suppl 1):23-30.
21. Maki K, Inou N, Takanishi A, Miller AJ. Computer-assisted simulations in orthodontic diagnosis and the application of a new cone beam x-ray computed tomography. Orthod Craniofac Res 2003;6(Suppl 1):95-101.
22. Baumrind S, Carlson S, Beers A, Curry S, Norris K, Boyd RL. Using three-dimensional imaging to assess treatment outcomes in orthodontics: a progress report from the University of the Pacific. Orthod Craniofac Res 2003;6(Suppl 1):132-42.
23. Aboudara CA, Hatcher D, Nielsen IL, Miller A. A three-dimensional evaluation of the upper airway in adolescents. Orthod Craniofac Res 2003;6(Suppl 1):173-5.
24. Danforth RA, Dus I, Mah J. 3-D volume imaging for dentistry: a new dimension. J Calif Dent Assoc 2003;31:817-23.
25. Lascala CA, Panella J, Marques MM. Analysis of the accuracy of linear measurements obtained by cone beam computed tomography (CBCT-NewTom). Dentomaxillofac Radiol 2004;33:291-4.
26. Marmulla R, Wortche R, Muhling J, Hassfeld S. Geometric accuracy of the NewTom 9000 cone beam CT. Dentomaxillofac Radiol 2005;34:28-31.
27. Tsiklakis KK, Syriopoulos K, Stamatakis HC. Radiographic examination of the temporomandibular joint using cone beam computed tomography. Dentomaxillofac Radiol 2004;33:196-201.
28. Beason R, Brooks SL. TMJ imaging accuracy using alpha prototype of DentoCAT cone-beam CT [abstract]. J Dent Res 2004;83(Spec Iss A):1938.
29. Honda K, Arai Y, Kashima M, Takano Y, Sawada K, Ejima K, et al. Evaluation of the usefulness of the limited cone-beam CT (3DX) in the assessment of the thickness of the roof of the glenoid fossa of the temporomandibular joint. Dentomaxillofac Radiol 2004;33:391-5.
30. Honda K, Larheim TA, Johannessen S, Arai Y, Shinoda K, Westesson PL. Ortho cubic super-high resolution computed tomography: a new radiographic technique with application to the temporomandibular joint. Oral Surg Oral Med Oral Pathol Oral Radiol Endod 2001;91:239-43.
31. Hilgers ML, Scarfe WC, Scheetz JP, Farman AG. Accuracy of linear temporomandibular joint measurements with cone beam computed tomography and digital cephalometric radiography. Am J Orthod Dentofacial Orthop 2005;128:803-11.
32. Farman, AG, Scarfe WC, Hilgers MJ, Bida O, Moshiri M, Sukovic P. Dentomaxillofacial cone-beam CT for orthodontic assessment. In: Lemke HU, Inamura K, Doi K, Vannier MK, Farman AG, editors. Computer assisted radiology and surgery. Proceedings of the 19th International Congress on Computer Assisted Radiology and Surgery, Berlin, Germany, June 22–25, 2005. Amsterdam: Elsevier; 2005. p.1187-90. ISBN:0-444-51872-X.
33. Schuytser FA, Van Cleynenbreugel J. From 3-D volumetric computer tomography to 3-D cephalometry. In: Swennen GJ, Schuytser FA, Hausamen JE, editors. Three dimensional cephalometry: a color atlas and manual. Berlin: Springer GmbH; 2005. p. 2-11. ISBN: 3-540-25440-4.
34. Scarfe WC, Farman AG, Sukovic P. Clinical applications of cone beam computed tomography in dental practice. J Can Dent Assoc 2006;72:75-80.
35. Farman AG, Scarfe WC. Development of imaging selection criteria and procedures should precede cephalometric assessment with cone-beam computed tomography. Am J Orthod Dentofacial Orthop 2006;130:257-65.
36. Chidiac JJ, Shofer FS, Al-Kutoub A, Laster LL, Ghafari J. Comparison of CT scanograms and cephalometric radiographs in craniofacial imaging. Orthod Craniofac Res 2002;5:104-13.
37. Farman AG. ALARA still applies. Oral Surg Oral Med Oral Pathol Oral Radiol Endod 2005;100:395-7.
38. Power G, Breckon J, Sherriff M, McDonald F. Dolphin imaging software: an analysis of the accuracy of cephalometric digitization and orthognathic prediction. Int J Oral Maxillofac Surg 2005;34:619-26.
39. Malkoc S, Sari Z, Usumez S, Koyuturk AE. The effect of head rotation on cephalometric radiographs. Eur J Orthod 2005;2:315-21.
40. Yoon YJ, Kim DH, Yu PS, Kim HJ, Choi EH, Kim KW. Effect of head rotation on posteroanterior cephalometric radiographs. Angle Orthod 2002;72:36-42.
41. Tsao DH, Kazanoglu A, McCasland JP. Measurability of radiographic images. Am J Orthod 1983;84:212-6.

42. Tsao DH. Graphic description of figure representation of the teeth and mandible in centric occlusion. J Prosthet Dent 1982;47:95-100.
43. Adams GL, Gansky SA, Miller AJ, Harrell WE Jr, Hatcher DC. Comparison between traditional 2-dimensional cephalometry and a 3-dimensional approach on human dry skulls. Am J Orthod Dentofacial Orthop 2004;126:397-409.
44. Feldkamp LA, Davis LC, Kress JW. Practical cone-beam algorithm. J Opt Soc Am 1984;1:612-9.
45. Kamoen A, Dermaut L, Verbeeck R. The clinical significance of error measurement in the interpretation of treatment results. Eur J Orthod 2001;23:569-78.
46. Cooke MS, Wei SH. Cephalometric errors: a comparison between repeat measurements and retaken radiographs. Aust Dent J 1991;36:38-43.
47. Mori Y, Miyajima T, Minami K, Sakuda M. An accurate three-dimensional cephalometric system: a solution for the correction of cephalic malpositioning. J Orthod 2001;28:143-9.
48. Perillo M, Beideman R, Shofer F, Jacobsson-Hunt U, Higgins-Barber K, Laster L, et al. Effect of landmark identification on cephalometric measurements: guidelines for cephalometric analyses. Clin Orthod Res 2000;3:29-36.
49. Held CL, Ferguson DJ, Gallo MW. Cephalometric digitization: a determination of the minimum scanner settings necessary for precise landmark identification. Am J Orthod Dentofacial Orthop 2001;119:472-81.
50. Halazonetis DJ. At what resolution should I scan cephalometric radiographs? Am J Orthod Dentofacial Orthop 2004;125: 118-9.